Formation Planning for Tethered Multirotor UAV Cooperative Transportation with Unknown Payload and Cable Length

Xiaozhen Zhang, Fan Zhang, *Member, IEEE,* and Panfeng Huang, *Senior Member, IEEE*

***Abstract*—This study investigates the formation planning problem of tethered multirotor unmanned aerial vehicle (UAV) cooperative transportation with unknown payload and cable length. Normally, the transportation formation and trajectory are given in advance or designed based on the coupled system model. It is challenging to dynamically generate flexible formations in response to changing environments when the payload and cable length are unknown. This paper proposes an online formation planning method for multirotor UAVs. First, by analyzing the tension on cables, we propose some formation criteria and further construct a corresponding performance function of optimization. Then, desired trajectories/formations that can reduce the cost functions are generated by using the admittance model. Next, an estimation-based formation tracking control is designed, which ensures that multirotor UAVs follow the desired trajectories/formations. Finally, numerical simulations and experiments are conducted to demonstrate the effectiveness of the proposed method.**

***Note to Practitioners*—This paper is motivated by the formation planning problem of tethered multirotor UAV cooperative transportation. In industry and production applications, a team of multirotor UAVs has a larger load capacity than a single one. Nevertheless, the formation planning of the tethered cooperative transportation is challenging, especially when the payload and cable length are unknown. Rather than give a predefined formation or trajectory, this paper suggests an online formation planning method for multirotor UAVs in case of unknown payload and cable length. The method is implemented through the following three parts: 1) By analyzing the tension on cables, we propose some formation criteria and further construct a corresponding performance function of optimization. 2) By using the admittance model, we generate desired trajectories/formations that can minimize the proposed cost function. 3) By estimating cable tension, we design formation tracking control laws for multirotor UAVs to follow the desired trajectories/formations. The proposed formation planning method does not rely on the knowledge of the payload and length of cables, which makes it can be easily applied to extensive industry, production, and military practice. Finally, numerical simulations and experiments are conducted to demonstrate the feasibility of the proposed method.**

***Index Terms*—Aerial cooperative system, cooperative transportation, formation planning, admittance control.**

I. Introduction

A. Motivation

COLLABORATIVE work is usually more effective than a single individual. Multirotor unmanned aerial vehicle (UAV) is considered to be a powerful air platform [1]. In recent years, there have been growing applications of multi-UAV cooperative operation in kinds of fields, including surveillance [2]-[3], fixed-wing recovery [4]-[5], forest firefighting [6]. Cooperative aerial transportation has also attracted the interest of many researchers. Employing multiple multirotor UAVs can enlarge the load capacity and manipulate heavier payloads.

Tethered multirotor UAV cooperative transportation system composes of a group of multirotor UAVs and a cable-suspended payload. Since multirotor UAVs connect to the same payload using cables, this cooperative transportation system is generally recognized to have a coupled complex dynamics model. However, it is difficult to establish such coupled model when the payload and cable length are unknown. Model-based formation planning methods are no longer applicable. Therefore, the motivation of this paper is to investigate a formation planning method for tethered multirotor UAV cooperative transportation with unknown payload and cable length.

B. Related Work

The tethered multirotor UAV cooperative transportation system is similar to the cable-driven parallel robot [7] in structure. Based on this characteristic, in [8]-[9], the authors propose attitude and position control schemes for the 6-degree of freedom (DOF) rigid body payload by analyzing inverse kinematics. In [10]-[11], the authors design a feedback control for the payload to obtain desired input of the payload, and then distribute optimal input to each tethered cable by solving an optimization problem. Thapa *et al.* in [12]-[13] propose an adaptive decentralized control method for trajectory tracking of the payload with unknown mass. Lee proposes a geometric control method for a point-mass payload [14] and a 6-DOF rigid body payload [15]-[16], where the minimum-norm solution is used to obtain the desired tension on cables.

All of the above control methods [7]-[16] require some system models. However, when the payload and cable length are unknown, it is hard to establish the coupled system model, and these model-based methods are hardly effective. Thereby, some studies [17]-[22] attempt not to use the coupling model. They regard tension on cables as the external disturbance for multirotor UAVs. The control objective is shifted to maintaining an appropriate formation of multirotor UAVs

This work was supported in part by the National Natural Science Foundation of China under Grant Nos. 62222313, and 62173275. (Corresponding author: *Panfeng Huang*.)

Authors are with the National Key Laboratory of Aerospace Flight Dynamics, Research Center for Intelligent Robotics, School of Astronautics, Northwestern Polytechnical University, 127 West Youyi Road, Xian, China (e-mail: jiaozhen@mail.nwpu.edu.cn, fzhang@nwpu.edu.cn, pfhuang@nwpu.edu.cn).

under tension disturbance. The tension disturbance can be handled by sensor measurements [17], integral terms [18], robustness of single UAVs [19], disturbance observer [20]-[21], and INDI controller [22]. However, pre-designed mission formations/trajectories are always required for the formation tracking of multirotor UAVs.

The compliance control methods (impedance and admittance control) have been applied to the multi-robot cooperative transportation system. [23] presents a leader-follower-based impedance control for underwater vehicles' cooperative manipulator transportation system, where no explicit data exchanging is required, and the cooperative information relies on the interaction force and torque measurements. In [24]-[25], admittance control method is used in dual multirotor UAVs cooperative transportation, where UAVs are directly attached to the payload. Tagliabue extends the results to the case of more multirotor UAVs [26]. In [27], Gabellieri *et al.* propose an admittance control scheme for a team of tethered multirotor UAVs using a leader-follower structure, but collisions are not considered. In [28]-[30], the potential field method is used for collision avoidance in tethered dual multirotor UAVs cooperative transportation. In [31], the authors developed a control barrier function to handle the obstacle avoidance problem. In [32]-[33], the cooperative obstacle avoidance problem is taken into the model predictive control framework, where the formation of UAVs is generated by optimization. Although the above studies [24]-[33] can generate feasible formations of multirotor UAVs for cooperative transportation, exact model information is required. When the payload and cable length are unknown, these methods can hardly work.

C. Contribution

This paper proposes an online formation planning method for tethered multirotor UAV cooperative transportation system. The proposed method can work without knowing the payload and cable length. First, we analyze the tension magnitude on cables in the transportation system, and propose some formation criteria. According to the proposed criteria, a corresponding performance function of optimization is constructed. Then, we consider the admittance model for governing the dynamics of the desired positions of multirotor UAVs, and simultaneously minimize the tension- and position-dependent cost functions. Next, an estimation-based control scheme for multirotor UAVs is addressed to track the generated desired formation/trajectories under tension disturbance.

The main contributions of this study are summarized as follows:

1) For the dynamic maneuvering of the cooperative transportation, we propose some formation criteria, which are independent of payload and cable length. It allows us to draft the desired transportation formation without knowing the payload and cable length. Compared with model-based planning methods [33]-[32], the proposed method is applicable to a more extensive range of scenarios.

2) Corresponding to the proposed criteria, we construct the performance function of optimization, which is solved online so that the proposed formation planning method can cope with dynamic environments.

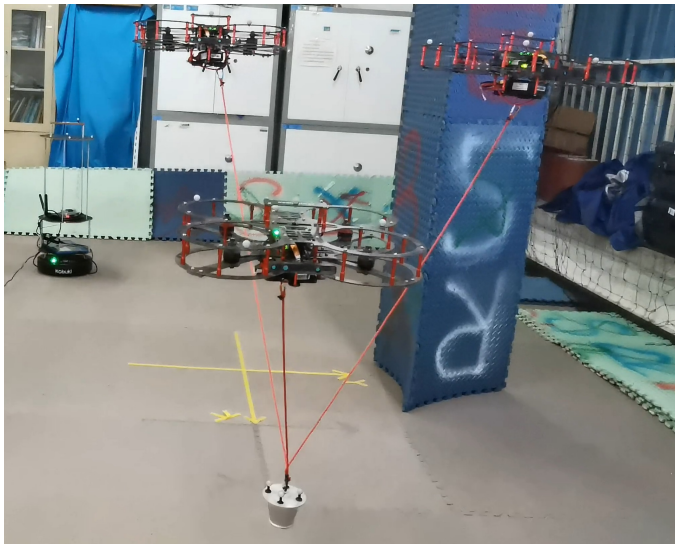

Fig. 1. Hardware experiment with three tethered quadrotor UAVs cooperative transportation.

3) By employing the admittance model, the proposed method can well maintain tension on cables, meanwhile, achieve obstacle avoidance and cooperative transportation. The maintenance of cable tension is neglected by many existing studies [29], [32]-[33].

4) The proposed admittance-based formation planning method is designed for point-mass payloads, which are more complex than bar payloads [24]-[26]. For the bar payload, it is only necessary to keep the horizontal component of tension on each cable as zero to form a feasible formation. However, for the point-mass payload, the formation when the horizontal component of tension on each cable is zero will lead to collisions of multirotor UAVs, so the tethered cables need to be inclined to maintain safe distances.

D. Organization

The remainder of this paper is organized as follows. First, the dynamics model of multirotor UAVs and the formation planning problem are addressed in Section II. The formation planning method for tethered multirotor UAV cooperative transportation is described in Section III. Section IV describes an estimation-based formation tracking control to track the generated desired formation under cable tension. Finally, the simulations and experiments conducted to verify the proposed design method are discussed in Section V and Section VI.

II. System Description and Problem Statement

A. System Description

As shown in Fig. 1, the tethered multirotor UAV cooperative transportation system is composed of $n\,(n \geq 3)$ same multirotor UAVs and a point-mass payload. There are *n* cables connecting the payload and centroid of UAVs.

In the inertial frame, the position of the *i*th multirotor UAV is denoted by $\boldsymbol{p}_i = \begin{bmatrix} x_i & y_i & z_i \end{bmatrix}^{\mathrm{T}}$. In body frame of the *i*th multirotor UAV, whose attitude is denoted by

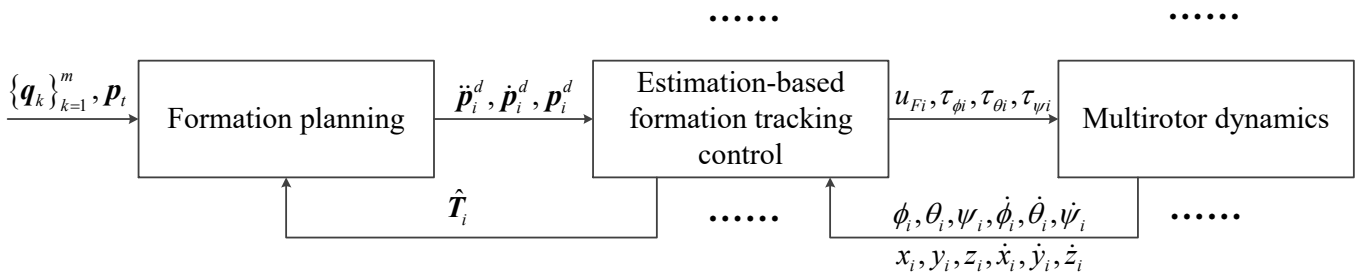

Fig. 2. Framework of planning and control for tether multirotor UAV cooperative transportation.

$\boldsymbol{\chi}_i = \begin{bmatrix}\phi_i & \theta_i & \psi_i\end{bmatrix}^{\mathrm{T}}$. ϕ_i, θ_i, and ψ_i represent the roll, pitch, and yaw, respectively. The dynamics of *i*th multirotor UAV is given as follows [34]-[35].

$$\ddot{x}_i = \frac{(\cos\phi_i \sin\theta_i \cos\psi_i + \sin\psi_i \sin\psi_i)u_{Fi} - T_{xi}}{m_i}, \quad (1a)$$

$$\ddot{y}_i = \frac{(\cos\phi_i \sin\theta_i \sin\psi_i + \sin\psi_i \cos\psi_i)u_{Fi} - T_{yi}}{m_i}, \quad (1b)$$

$$\ddot{z}_i = \frac{u_{Fi}\cos\phi_i \cos\theta_i - T_{zi}}{m_i} + g, \quad (1c)$$

$$\ddot{\phi}_i = \frac{\dot{\theta}_i\dot{\psi}_i(I_y - I_z)}{I_x} + \frac{\tau_{\phi i}}{I_x}, \quad (1d)$$

$$\ddot{\theta}_i = \frac{\dot{\psi}_i\dot{\phi}_i(I_z - I_x)}{I_y} + \frac{\tau_{\theta i}}{I_y}, \quad (1e)$$

$$\ddot{\psi}_i = \frac{\dot{\phi}_i\dot{\theta}_i(I_x - I_y)}{I_z} + \frac{\tau_{\psi i}}{I_z}, \quad (1f)$$

where u_{Fi} represents the magnitude of thrust; $\boldsymbol{\tau}_i = \begin{bmatrix}\tau_{\phi i} & \tau_{\theta i} & \tau_{\psi i}\end{bmatrix}^{\mathrm{T}}$ is the the control torque. I_x, I_y, and I_z are the rotational inertia. g is the gravitational acceleration. $\boldsymbol{T}_i = \begin{bmatrix}T_{xi} & T_{yi} & T_{zi}\end{bmatrix}^{\mathrm{T}}$ represents the tension, whose direction is defined as from the payload to the *i*th multirotor UAV.

Typically, (1a)-(1c) describe the position motion of a multirotor UAV, and thus called position dynamics. (1d)-(1f) describe the attitude motion of a multirotor UAV, and thus called attitude dynamics.

B. Problem Statement

The primary objective of this study is to generate flexible formations for tethered multirotor UAVs to cooperatively transport the payload to the target in obstacle environments. An important condition is that the payload and cable length are unknown, which means the height between multirotor UAVs and the payload (or rather the height of the transportation system) is also unknown. Thus, obstacle avoidance is considered in the 2-dimensional xOy plane. We have some definitions as follows:

Obstacle: There are *m* static or dynamic cylindrical obstacles in transportation environment. The *k*th obstacle is defined as a circle with the center at $\boldsymbol{q}_k = \begin{bmatrix}x_k & y_k\end{bmatrix}^{\mathrm{T}}$ and the radius of r_k.

2D Position of Multirotor UAV: $\boldsymbol{w}_i^d = \begin{bmatrix}x_i^d & y_i^d\end{bmatrix}^{\mathrm{T}}$ represents the desired 2D position of the *i*th UAV in xOy plane.

Transportation Target: $\boldsymbol{p}_t = \begin{bmatrix}x_t & y_t & z_t\end{bmatrix}^{\mathrm{T}}$ is the unique transportation target location, and $\boldsymbol{w}_t = \begin{bmatrix}x_t & y_t\end{bmatrix}^{\mathrm{T}}$ represents the 2D position of target in xOy plane.

Fig. 2 shows the framework of the proposed formation planning method, where obstacles, the transportation target, and tension estimation are informed to the formation planning, which generates a continue desired formation $\{\boldsymbol{p}_i^d\}_{i=1}^n$. Then, multirotor UAVs track the formation using an estimation-based formation tracking control scheme under tension disturbance. The designed estimator can provide the cable tension measurement $\hat{\boldsymbol{T}}_i$, which is also useful in formation planning.

III. Formation Planning

This section describes the formation planning method for tethered multirotor UAV cooperative transportation system with unknown payload and cable length. First, we propose some formation criteria, which is independent of the payload and cable length. Then, corresponding to the proposed criteria, we construct a cost function for optimization. Finally, we employ an admittance model to minimize the proposed cost function, generating desired formation/trajectories for further position tracking control.

A. Formation criteria

In this subsection, we propose the following formation criteria for cooperative transportation:

1) Balance the multirotor UAVs' contribution to payload transportation.
2) Swarm reciprocal avoidance.
3) Obstacle avoidance.

Swarm reciprocal avoidance and obstacle avoidance are two general requirements in formation planning. Balancing the multirotor UAVs' contribution to payload transportation represents equalizing tension magnitude on tethered cables.

It is remarked that criterion 1) is related to the tension on cables; Criteria 2) and 3) are related to the position of multirotor UAVs. Thereby, the proposed formation criteria are independent of the payload and cable length. This is the basis for achieving formation planning with unknown payload and cable length.

In [38] and [39], similar considerations with criterion 1) for tension magnitude can also be found. In the following, we will explain the necessity of criterion 1) for cooperative transportation. We first introduce the asymmetry tension here.

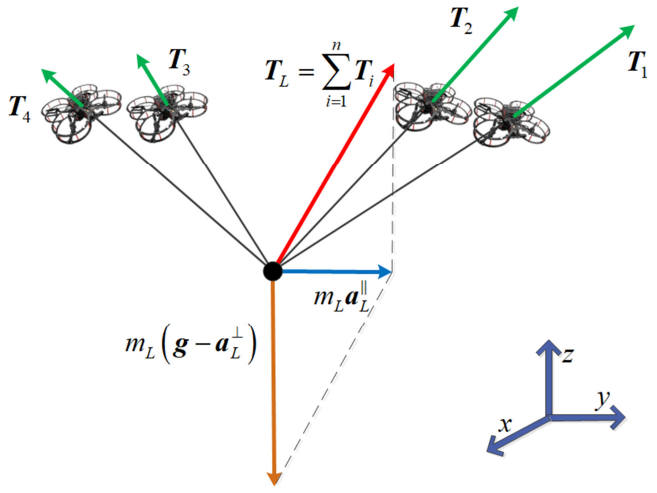

Fig. 3. Acceleration of multi-UAV cooperative transportation system.

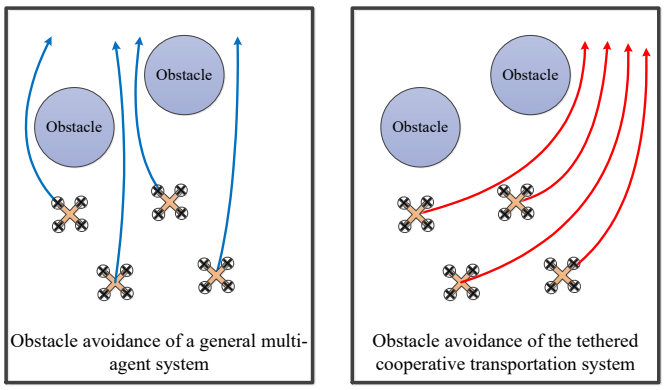

Fig. 4. The obstacle avoidance of a general multi-agent system enables bypassing from both sides of one obstacle (Fig. 4 left). However, in the tethered cooperative transportation system, due to the tethered cables, the behavior in Fig. 4 left is not allowed. The overall obstacle avoidance behavior is acceptable (Fig. 4 right).

Asymmetric Tension: The asymmetric tension means that the tension magnitudes on cables are different, such that $\Gamma_i \neq \Gamma_j,\ \exists\ i, j$, where $\Gamma_i = \|\boldsymbol{T}_i\|_2$.

For the payload with the mass of m_L, the force equilibrium is given by

$$m_L \boldsymbol{a}_L = m_L \boldsymbol{g} + \sum_{i=1}^{n} \boldsymbol{T}_i, \tag{2}$$

where $\boldsymbol{a}_L = \boldsymbol{a}_L^{\parallel} + \boldsymbol{a}_L^{\perp}$ represents the acceleration of the payload; $\boldsymbol{a}_L^{\parallel} = \begin{bmatrix} * & * & 0 \end{bmatrix}^T$ is the horizontal component of $\boldsymbol{a}_L$; $\boldsymbol{a}_L^{\perp} = \begin{bmatrix} 0 & 0 & * \end{bmatrix}^T$ is the vertical component of $\boldsymbol{a}_L$.

It can be divided into two categories according to the value of $\boldsymbol{a}_L^{\parallel}$.

Case I, $\boldsymbol{a}_L^{\parallel} = \boldsymbol{0}$: $\boldsymbol{a}_L^{\parallel} = \boldsymbol{0}$ implies the transportation system is static hovering or travelling at a uniform speed. If asymmetric tension appears, one multirotor UAV will have high output with high tension magnitude, while the other one will have low output. High tension magnitude is associated with high power consumption, and its tethered UAV will have dead batteries first. Thereby, asymmetric tension is adverse to the endurance of the cooperative transportation system.

Case II, $\boldsymbol{a}_L^{\parallel} \neq \boldsymbol{0}$: $\boldsymbol{a}_L^{\parallel} \neq \boldsymbol{0}$ implies the transportation system is accelerating or decelerating. If the system maintains a fixed formation, it can easily lead to asymmetric tension. In Fig. 3, for example, due to the horizontal acceleration $\boldsymbol{a}_L$, tension magnitude on cables are not equal, namely $\Gamma_1 > \Gamma_4$. According to (2), for the larger acceleration, the magnitude of Γ_1 and Γ_2 are required to increase for a larger horizontal component. It is easy to reach the power limit of an individual UAV. Thereby, asymmetric tension is adverse to the acceleration and deceleration performance of cooperative transportation.

B. Formation Optimization

In this subsection, corresponding to the proposed criteria in Section III-A, a cost function is constructed as follows:

$$J\left(\hat{\Gamma}_1, \ldots, \hat{\Gamma}_n, \boldsymbol{p}_1^d, \ldots, \boldsymbol{p}_n^d\right) = J_1 + J_2, \tag{3}$$

with

$$J_1 = \frac{1}{2n} \sum_{i=1}^{n} \sum_{j=1}^{n} \left(\hat{\Gamma}_i - \hat{\Gamma}_j\right)^2,$$

$$J_2 = \sum_{i=1}^{n} \sum_{j=1}^{n} V_{ij}\left(\boldsymbol{p}_i^d, \boldsymbol{p}_j^d\right) + (1-c) \sum_{i=1}^{n} \sum_{k=1}^{m} V_{\text{obs}}\left(\boldsymbol{w}_i^d, \boldsymbol{q}_k\right) + cn\left[V_{\text{tar}}\left(\boldsymbol{p}_c^d, \boldsymbol{p}_t\right) + \sum_{k=1}^{m} V_{\text{obs}}\left(\boldsymbol{w}_c^d, \boldsymbol{q}_k\right)\right],$$

where V_{ij}, V_{tar}, and V_{obs} are potential functions for safe flight distance, transportation target guidance, and obstacle avoidance, respectively; $\hat{\Gamma}_i$ denotes the measured tension magnitude; $\boldsymbol{p}_i^d$ represents the desired position of ith UAV. Parameter $0 < c < 1$ is the weight to adjust the policies of individual UAVs and the overall team. Large c implies strengthening overall team policy. Small c means the emphasis on individual policies. $\boldsymbol{p}_c^d$ is the position of the UAVs team (or the position of the system), which can be computed by $\boldsymbol{p}_c^d = \begin{bmatrix} x_c & y_c & z_c \end{bmatrix}^{\mathrm{T}} = \frac{1}{n} \sum_{i=1}^{n} \boldsymbol{p}_i^d$; $\boldsymbol{w}_c = \begin{bmatrix} x_c & y_c \end{bmatrix}^{\mathrm{T}}$ is the 2D position of the UAVs team.

In (3), J_1 corresponds to criterion 1) for suppressing asymmetric tension; J_2 corresponds to criteria 2) and 3) for swarm reciprocal avoidance, obstacle avoidance, and transportation target.

In the proposed cost J_2, obstacle avoidance is considered not only for each single multirotor UAV, but also for the overall transportation system, denoted by $V_{\text{obs}}\left(\boldsymbol{w}_i^d, \boldsymbol{q}_k\right)$ and $V_{\text{obs}}\left(\boldsymbol{w}_c^d, \boldsymbol{q}_k\right)$, respectively. Different from general multi-agent systems, UAVs in the cooperative transportation system are tethered and share the same transportation target. As shown in Fig. 4, The case that UAVs bypass from both sides of one obstacle can be avoided by the increasing parameter c to emphasize the overall obstacle avoidance. The case in Fig. 4 right is preferred.

Remark 1: In the tethered aerial cooperative transportation system, to maintain proper safe flight distances, cables are inclined. The xOy position of the payload will fall in the convex polygon of UAVs. Therefore, obstacle avoidance of

UAVs is sufficient for the transportation system. It is also remarked that our formation is dynamic, when the system is accelerating. If cables are excessively long, the xOy position of the payload may move beyond the convex polygon. However, excessively long cables are likely to result in poor static stability of the transportation system [44]-[45], so the configured practical tethered cooperative transportation system should avoid excessively long cables.

C. Admittance Model for Formation Generation

In this subsection, the desired position of multirotor UAVs will be generated by the admittance model.

It is started from the classical virtual spring-mass-damper model for each UAV [40]-[41]:

$$M_d\left(\ddot{\boldsymbol{p}}_i^d-\ddot{\boldsymbol{p}}_i^f\right)+D_d\left(\dot{\boldsymbol{p}}_i^d-\dot{\boldsymbol{p}}_i^f\right)+K_d\left(\boldsymbol{p}_i^d-\boldsymbol{p}_i^f\right)=\boldsymbol{F}_i^d, \quad (4)$$

where M_d represents the inertia, D_d is the damping coefficient and K_d is the stiffness coefficient. $\boldsymbol{p}_i^f$, and $\boldsymbol{p}_i^d$ are the reference position and the desire position of *i*th UAV in the inertial frame. $\boldsymbol{F}_i^d$ is the desired force acting on the UAV to be designed.

We define $K_d=0$, and $\ddot{\boldsymbol{p}}_i^f=\dot{\boldsymbol{p}}_i^f=\boldsymbol{0}$ in (4). $K_d=0$ represents the force interaction is fully compliant. In our method, there is no predefined reference position. $\ddot{\boldsymbol{p}}_i^f=\dot{\boldsymbol{p}}_i^f=\boldsymbol{0}$ represent that the reference position is an unknown stationary point.

Then, (4) can be rewritten as

$$\ddot{\boldsymbol{p}}_i^d=k_1\boldsymbol{F}_i^d-k_2\dot{\boldsymbol{p}}_i^d, \quad (5)$$

where $k_1=1/M_d>0$ and $k_2=D_d/M_d>0$. (5) is the utilized admittance model, which describes the dynamics of the desired position $\boldsymbol{p}_i^d$.

We divide $\boldsymbol{F}_i^d$ into two parts:

$$\boldsymbol{F}_i^d=\boldsymbol{F}_{1i}^d+\boldsymbol{F}_{2i}^d, \quad (6)$$

where $\boldsymbol{F}_{1i}^d$ is designed to reduce cost J_1, $\boldsymbol{F}_{2i}^d$ is designed to reduce cost J_2.

We know if $\hat{\Gamma}_i=\hat{\Gamma}_{ave}\triangleq\frac{1}{n}\sum_{j=1}^n\hat{\Gamma}_j$ for $\forall i$, J_1 has the minimum. Therefore, to minimize J_1, the desired tension magnitude on *i*th cable is designed to be $\hat{\Gamma}_{ave}$. The current tension on the *i*th cable is $\hat{\Gamma}_i$. And thus it requires the tension magnitude to change $\hat{\Gamma}_{ave}-\hat{\Gamma}_i$. We also know the cable tension is always along the cable. Thereby, $\boldsymbol{F}_{1i}^d$ is designed as

$$\boldsymbol{F}_{1i}^d=\boldsymbol{v}_i\left(\hat{\Gamma}_{ave}-\hat{\Gamma}_i\right), \quad (7)$$

where $\boldsymbol{v}_i=-\frac{\boldsymbol{T}_i}{\hat{\Gamma}_i}$ represents the direction of cable tension. $\boldsymbol{F}_{1i}^d$ represents the desired variation of the interaction force between the cable and multirotor UAV. The admittance model (5) can convert force error into deviation of relative desired displacement through position control that will be described in the next section.

J_2 is related to the desired position of multirotor UAVs. To minimize J_2, we can let the desired position follow the gradient descent direction $\Delta\boldsymbol{p}_i^d$:

$$\Delta\boldsymbol{p}_i^d=-\nabla_{\boldsymbol{p}_i^d}J_2. \quad (8)$$

The objective becomes to track the velocity $\Delta\boldsymbol{p}_i^d$. The feedback control for the system (5) is design as

$$\boldsymbol{F}_{2i}^d=-k_3\left(\dot{\boldsymbol{p}}_i^d-\Delta\boldsymbol{p}_i^d\right). \quad (9)$$

So far, we know the designed $\boldsymbol{F}_{1i}^d$ and $\boldsymbol{F}_{2i}^d$ can reduce the cost J_1 and J_2, respectively. Now let's consider the formations at the minimum of J_1 and J_2, respectively.

Define the formation set $\{\boldsymbol{p}_{1i}^*\}_{i=1}^n$ corresponding to the minimum J_1, where $\hat{\Gamma}_i=\hat{\Gamma}_j=\hat{\Gamma}_{ave}$, $\forall i,j$. Thus, according to the force equilibrium (2), it has

$$\begin{aligned}&\{\boldsymbol{p}_{1i}^*\}_{i=1}^n\\&=\left\{m_L\boldsymbol{a}_L^*=m_L\boldsymbol{g}+\sum_{i=1}^n\frac{\boldsymbol{p}_{1i}^*-\boldsymbol{p}_L^*}{||\boldsymbol{p}_{1i}^*-\boldsymbol{p}_L^*||_2}\hat{\Gamma}_{ave},\ \boldsymbol{p}_{1i}^*\in\mathbb{R}^3\right\},\end{aligned} \quad (10)$$

where $\boldsymbol{p}_L^*$ and $\boldsymbol{a}_L^*$ denotes the payload's position and acceleration, respectively, when J_1 is minimized. We can find that $\{\boldsymbol{p}_{1i}^*\}_{i=1}^n$ includes a series of formations, because the force equilibrium has multiple solutions. Moreover, $\{\boldsymbol{p}_{1i}^*\}_{i=1}^n$ can be translated in 3-dimensional space, with the translation of $\boldsymbol{p}_L^*$.

Define the formation set $\{\boldsymbol{p}_{2i}^*\}_{i=1}^n$ corresponding to the minimum J_2, which implies that the transportation system reaches the transportation target, such that $\frac{1}{n}\sum_{i=1}^n\boldsymbol{p}_{2i}^*=\boldsymbol{p}_t$. Therefore, it has

$$\{\boldsymbol{p}_{2i}^*\}_{i=1}^n=\left\{\frac{1}{n}\sum_{i=1}^n\boldsymbol{p}_{2i}^*=\boldsymbol{p}_t, V_2\left(\boldsymbol{p}_{2i}^*\right)=0,\ \boldsymbol{p}_{2i}^*\in\mathbb{R}^3\right\}, \quad (11)$$

where $V_2\left(\boldsymbol{p}_{2i}^*\right)$ includes the constructed potential functions V_{ij} and V_{obs} given in (3).

By comparing formation set $\{\boldsymbol{p}_{1i}^*\}_{i=1}^n$ and $\{\boldsymbol{p}_{2i}^*\}_{i=1}^n$, we find that their intersection is not empty. There exist a set of formation $\{\boldsymbol{p}_i^*\}_{i=1}^n=\{\boldsymbol{p}_{1i}^*\}_{i=1}^n\bigcap\{\boldsymbol{p}_{2i}^*\}_{i=1}^n$ corresponding to the minimized $J=J_1+J_2$. Therefore, the designed $\boldsymbol{F}_i^d=\boldsymbol{F}_{1i}^d+\boldsymbol{F}_{2i}^d$ can minimize the proposed cost J. It has

$$\{\boldsymbol{p}_i^*\}_{i=1}^n=\left\{\begin{array}{l}\boldsymbol{0}=m_L\boldsymbol{g}+\sum_{i=1}^n\frac{\boldsymbol{p}_{1i}^*-\boldsymbol{p}_L^*}{||\boldsymbol{p}_{1i}^*-\boldsymbol{p}_L^*||_2}\hat{\Gamma}_{ave},\\ \frac{1}{n}\sum_{i=1}^n\boldsymbol{p}_i^*=\boldsymbol{p}_t, V_2\left(\boldsymbol{p}_i^*\right)=0, \boldsymbol{p}_i^*\in\mathbb{R}^3\end{array}\right\}. \quad (12)$$

This set of formations $\{\boldsymbol{p}_i^*\}_{i=1}^n$ is collision-free and near the transportation target, satisfying $\frac{1}{n}\sum_{i=1}^n\boldsymbol{p}_i^*=\boldsymbol{p}_t$. Further, the gravity of the payload is evenly distributed to all multirotor UAVs. It is remarked that the term $\boldsymbol{a}_L^*$ is disappeared in (12), because of the damping term $-k_2\dot{\boldsymbol{p}}_i^d$ in the dynamics (5). The cooperative transportation system will eventually be stationary.

In addition, it is noticed that (5) is a differential form, which associates with the initial value problem. The initial desired position can be selected as the initial position, such that $\boldsymbol{p}_i^d\left(0\right)=\boldsymbol{p}_i\left(0\right)$, and $\dot{\boldsymbol{p}}_i^d(0)=0$.

IV. Estimated-Based Formation Tracking Control

This section describes an estimation-based formation tracking control to track the generated desired formations (Section III). The framework of the control scheme is shown in

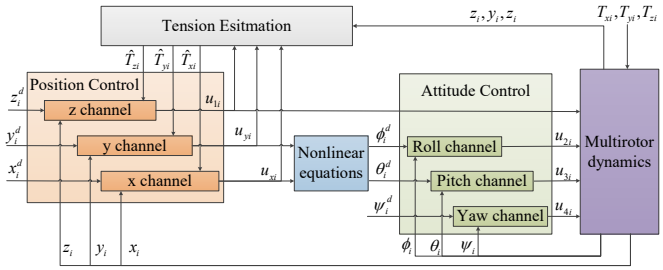

Fig. 5. Estimation-based formation tracking control framework of a single multirotor UAV.

Fig. 5. First, an observer is employed to estimate the tension on cables. Then, we proposed an attitude control and a tension estimation-based position control for multirotor UAVs.

The dynamic model of one multirotor UAV with tethered cable is given in (1a)-(1f). Multirotor UAV is an under-actuated system because there are four control inputs but six state variables. The horizontal control is closely related to the roll and pitch control. The desired roll angle and the desired pitch angle need to be solved from the horizontal control component, that is, the following nonlinear equations:

$$\begin{cases} u_{xi} = \cos\phi_i \sin\theta_i \cos\psi_i + \sin\psi_i \sin\psi_i \\ u_{yi} = \cos\phi_i \sin\theta_i \sin\psi_i + \sin\psi_i \cos\psi_i \end{cases}. \tag{13}$$

Solve (13), the desired attitude angle can be obtained as below:

$$\begin{cases} \phi_i^d = \arcsin\left(u_{xi}\sin\psi_i - u_{yi}\cos\psi_i\right) \\ \theta_i^d = \arcsin\left(\dfrac{u_{xi}\cos\psi_i - u_{yi}\sin\psi_i}{\cos\psi_i^d}\right) \end{cases}. \tag{14}$$

A. Tension Estimation

In the tethered aerial transportation system, the tension is caused by the interaction between the payload and multirotor UAVs, and is therefore bounded, such that

$$|\boldsymbol{T}_i| < \sigma_1, \quad \left|\dot{\boldsymbol{T}}_i\right| < \sigma_2, \quad \left|\ddot{\boldsymbol{T}}_i\right| < \sigma_3.$$

A disturbance observer modified from [48] is employed to estimate the tension on tethered cables:

$$\begin{cases} \hat{\boldsymbol{T}}_i = \boldsymbol{\xi}_{1i} + \mathbf{K}_1\left(\dot{\boldsymbol{p}}_i\right) \\ \dot{\boldsymbol{\xi}}_i = -\mathbf{L}_1\left(\dot{\boldsymbol{p}}_i\right)\left[m_i\ddot{\boldsymbol{p}}_u + \hat{\boldsymbol{T}}_i\right] + \dot{\hat{\boldsymbol{T}}}_i \\ \dot{\hat{\boldsymbol{T}}}_i = \boldsymbol{\xi}_{2i} + \mathbf{K}_2\left(\dot{\boldsymbol{p}}_i\right) \\ \dot{\boldsymbol{\xi}}_{2i} = -\mathbf{L}_2\left(\dot{\boldsymbol{p}}_i\right)\left[m_i\ddot{\boldsymbol{p}}_u + \hat{\boldsymbol{T}}_i\right] \end{cases}, \tag{15}$$

where $\hat{\boldsymbol{T}}_i = \begin{bmatrix}\hat{T}_{xi} & \hat{T}_{yi} & \hat{T}_{zi}\end{bmatrix}^{\mathrm{T}}$ is the estimation of tension $\boldsymbol{T}_i$. $m_i\ddot{\boldsymbol{p}}_u = \begin{bmatrix}u_{xi}u_{Fi} & u_{yi}u_{Fi} & u_{Fi}\cos\psi_i\cos\theta_i\end{bmatrix}^{\mathrm{T}}$ represents the gravity and control forces generated by each UAV. $\boldsymbol{\xi}_{1i}$ and $\boldsymbol{\xi}_{2i}$ are two auxiliary variables. $\mathbf{K}_1\left(\dot{\boldsymbol{p}}_i\right)$, $\mathbf{K}_2\left(\dot{\boldsymbol{p}}_i\right)$, $\mathbf{L}_1\left(\dot{\boldsymbol{p}}_i\right)$, and $\mathbf{L}_2\left(\dot{\boldsymbol{p}}_i\right)$ are the designed parameter matrices, satisfying

$$\begin{cases} \mathbf{L}_1\left(\dot{\boldsymbol{p}}_i\right) = \dfrac{\partial \mathbf{K}_1\left(\dot{\boldsymbol{p}}_i\right)}{\partial \dot{\boldsymbol{p}}} \\ \mathbf{L}_2\left(\dot{\boldsymbol{p}}_i\right) = \dfrac{\partial \mathbf{K}_2\left(\dot{\boldsymbol{p}}_i\right)}{\partial \dot{\boldsymbol{p}}} \end{cases}, \tag{16}$$

and

$$-\mathbf{L}\left(\dot{\boldsymbol{p}}_i\right) - 0.5||\boldsymbol{\gamma}||_2\mathbf{I}_6 > 0, \tag{17}$$

where

$$\mathbf{L}\left(\dot{\boldsymbol{p}}_i\right) = \begin{bmatrix}-\mathbf{L}_1\left(\dot{\boldsymbol{p}}_i\right) & \mathbf{I}_3 \\ \mathbf{L}_2\left(\dot{\boldsymbol{p}}_i\right) & \mathbf{0}_{3\times 3}\end{bmatrix}, \quad \boldsymbol{\gamma} = \begin{bmatrix}\mathbf{0}_{3\times 3} \\ \mathbf{I}_3\end{bmatrix}.$$

Theorem 1: With any $\mathbf{K}_1\left(\dot{\boldsymbol{p}}_i\right)$, $\mathbf{K}_2\left(\dot{\boldsymbol{p}}_i\right)$, $\mathbf{L}_1\left(\dot{\boldsymbol{p}}_i\right)$, and $\mathbf{L}_2\left(\dot{\boldsymbol{p}}_i\right)$ satisfying (16)-(17) for the estimator (15) and position dynamics (1a)-(1c) of one single multirotor UAV, the tension estimation error is bounded.

Proof: See Appendix A. ■

B. Tension Estimation-Based Position Control of Multirotor UAV

The tension estimation-based position control is designed as below:

$$\begin{cases} u_{xi} = \dfrac{m_i\left(\ddot{x}_i^d - r_x s_{xi} + c_x e_{xi}\right) + \hat{T}_{xi}}{u_{Fi}} \\ u_{yi} = \dfrac{m_i\left(\ddot{y}_i^d - r_y s_{yi} + c e_{yi}\right) + \hat{T}_{yi}}{u_{Fi}} \\ u_{Fi} = \dfrac{m_i\left(\ddot{z}_i^d - r_z s_{zi} + c_z \dot{e}_{zi} - g\right) + \hat{T}_{zi}}{\cos\phi_i\cos\theta_i} \end{cases}, \tag{18}$$

where $e_{xi} = x_i^d - x_i$, $e_{yi} = y_i^d - y_i$, and $e_{zi} = z_i^d - z_i$ are position tracking errors. $s_{xi} = c_x e_{xi} + \dot{e}_{xi}$, $s_{yi} = c_y e_{yi} + \dot{e}_{yi}$, and $s_{zi} = c_z e_{zi} + \dot{e}_{zi}$ are designed sliding mode surfaces. $\mathbf{R}_p = diag\left(r_x, r_y, r_z\right)$ and $\mathbf{C}_p = diag\left(c_x, c_y, c_z\right)$ are two positive define gain matrices.

Theorem 2: For the position dynamics of the multirotor UAV (1a)-(1c), if $\mathbf{R}_p$, $\mathbf{C}_p$, and $\mathbf{R}_p - 0.5\mathbf{I}_3$ are positive define, and the condition (19) is satisfied, the position tracking error (e_{xi}, e_{yi}, e_{zi}) are stable under the position control (18).

$$-\mathbf{L}\left(\dot{\boldsymbol{p}}_i\right) - 0.5||\boldsymbol{\gamma}||_2\mathbf{I}_6 - \frac{1}{2m_i}\mathbf{I}_6 > 0. \tag{19}$$

Proof: See Appendix B. ■

C. Attitude Control of Multirotor UAV

The attitude control is designed as below:

$$\begin{cases} \tau_{\phi i} = \left(\ddot{\phi}_i^d - r_\phi s_{\phi i} - c_\phi \dot{e}_{\phi i}\right) I_x - \left(I_y - I_z\right)\dot{\theta}_i\dot{\psi}_i \\ \tau_{\theta i} = \left(\ddot{\theta}_i^d - r_\theta s_{\theta i} - c_\theta \dot{e}_{\theta i}\right) I_y - \left(I_z - I_x\right)\dot{\psi}_i\dot{\phi}_i \\ \tau_{\psi i} = \left(\ddot{\psi}_i^d - r_\psi s_{\psi i} - c_\psi \dot{e}_{\psi i}\right) I_z - \left(I_x - I_y\right)\dot{\phi}_i\dot{\theta}_i \end{cases}, \tag{20}$$

where $e_{\phi i} = \psi_i^d - \psi_i$, $e_{\theta i} = \theta_i^d - \theta_i$, and $e_{\psi i} = \psi_i^d - \psi_i$ are attitude tracking errors. $s_{\phi i} = c_\phi e_{\phi i} + \dot{e}_{\phi i}$, $s_{\phi i} = c_\phi e_{\phi i} + \dot{e}_{\phi i}$, and $s_{\phi i} = c_\phi e_{\phi i} + \dot{e}_{\phi i}$ are designed sliding mode surfaces. $\mathbf{R}_a = diag\left(r_\phi, r_\theta, r_\psi\right)$ and $\mathbf{C}_a = diag\left(c_\phi, c_\theta, c_\psi\right)$ are two positive define gain matrices.

Theorem 3: For the attitude dynamics of the multirotor UAV (1d)-(1f), if $\mathbf{R}_a$ and $\mathbf{C}_a$ are positive define, the attitude control (20) can enforce the attitude track errors $(e_{\phi i}, e_{\theta i}, e_{\psi i})$ converge to zero.

Proof: See Appendix C. ■

V. Simulation

This section discusses the numerical simulations for tethered multirotor UAV cooperative transportation. Although the proposed methods do not rely on the information of the payload and cable length, a coupled system model is still required in the simulation platform to validate the proposed methods. The simulation platform constructs the coupled dynamics model of the cooperative transportation system using the Udwadia-Kalaba method ([33], or Appendix A of [47]). The desired formations/trajectories of multirotor UAVs are governed by the proposed planning method (5). Each UAV is deployed with the controller described in Section IV for desired formation tracking.

Two simulation scenarios are considered. The simulation with four multirotor UAVs will be analyzed in detail as follows, and the eight multirotor UAVs simulation may refer to the provided video.

A. Simulation Setup

It is considered that four 4kg multirotor UAVs collaboratively transport a 6kg payload in dynamic obstacles environment. The cables connecting the payload are 7.68m, 7.55m, 9.84m, and 8.66m in length, respectively. The initial desired formation and initial formation are the same. They are given as follows

$$\begin{cases} \boldsymbol{p}_1^d(0) = \boldsymbol{p}_1(0) = \begin{bmatrix} 5 & 3 & 5 \end{bmatrix}^{\mathrm{T}}\mathrm{m}, \\ \boldsymbol{p}_2^d(0) = \boldsymbol{p}_2(0) = \begin{bmatrix} 4 & -4 & 5 \end{bmatrix}^{\mathrm{T}}\mathrm{m}, \\ \boldsymbol{p}_3^d(0) = \boldsymbol{p}_3(0) = \begin{bmatrix} -6 & -6 & 5 \end{bmatrix}^{\mathrm{T}}\mathrm{m}, \\ \boldsymbol{p}_4^d(0) = \boldsymbol{p}_4(0) = \begin{bmatrix} -1 & 7 & 5 \end{bmatrix}^{\mathrm{T}}\mathrm{m}. \end{cases}$$

The initial position of the payload is $\boldsymbol{p}_L = \begin{bmatrix} 0 & 0 & 0 \end{bmatrix}^{\mathrm{T}}\mathrm{m}$. There are 6 static and dynamic cylindrical obstacles in the transportation environment with different radii. The transportation target is $\boldsymbol{p}_t = \begin{bmatrix} 12 & 70 & 7 \end{bmatrix}^{\mathrm{T}}\mathrm{m}$.

The parameters for formation planning are chosen as $k_1 = 1.4$, $k_2 = 15$, $k_3 = 1$, and $c = 0.5$. The parameters for tracking control are chosen as $\mathbf{K}_1(\dot{\boldsymbol{p}}_i) = \mathbf{K}_2(\dot{\boldsymbol{p}}_i) = 20\dot{\boldsymbol{p}}_i$, $\mathbf{C}_p = \mathbf{C}_a = diag(2,2,2)$, $\mathbf{R}_p = diag(1, 0.8, 0.8)$, and $\mathbf{R}_p = diag(5,5,5)$.

B. Simulation Results

As shown in Fig. 6 and 7, distinct formation changes exist when UAVs go through the dynamic obstacles environment, and static and dynamic obstacles are all avoided. The convex polygon consisting of UAVs is given in Fig. 7. It can be found that the payload is always inside the convex polygon, which implies the safety of the payload. Further, with the help of potential functions, collisions of multirotor UAVs are avoided. Fig. 8 shows that multirotor UAVs' distance is always kept within a feasible range. Fig. 8 also shows that the actual distance d_{ij} tracks the desired distance d_{ij}^d well, implying the effectiveness of position and attitude control.

The measured tension magnitude on cables from the tension estimator is presented in Fig. 9. Asymmetric tension exists at the beginning (t=0s). With the effect of $\boldsymbol{F}_{1i}^d$, cable tension magnitude reaches a consensus, eventually.

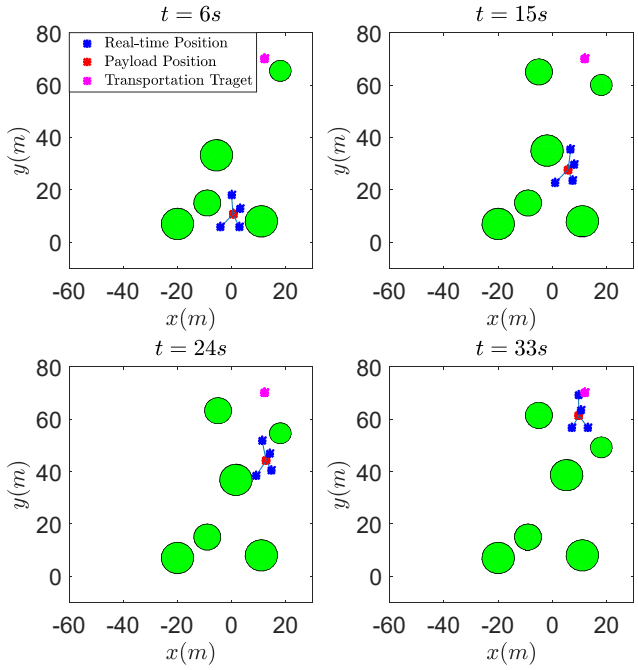

Fig. 6. The formation changes of UAVs during obstacles environment in the simulation.

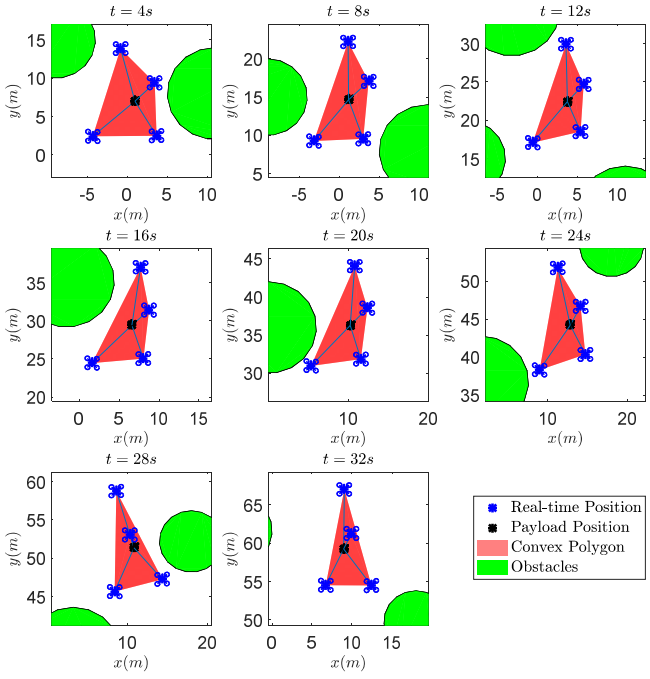

Fig. 7. The convex polygon of UAVs during obstacles environment in the simulation.

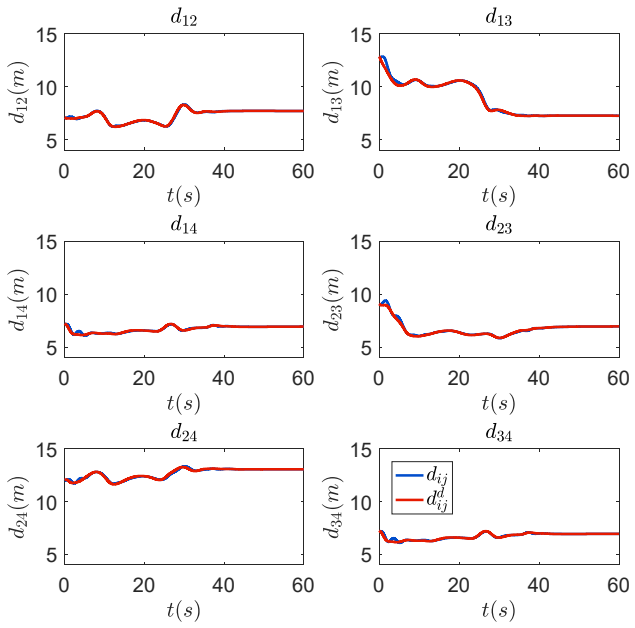

Fig. 8. The relative distance of UAVs in the simulation.

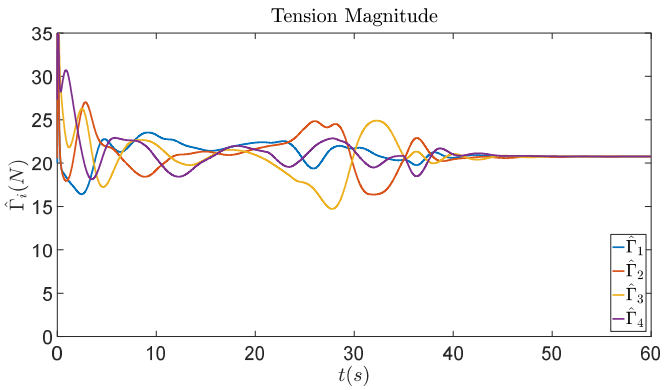

Fig. 9. The tension magnitude on cables in the simulation.

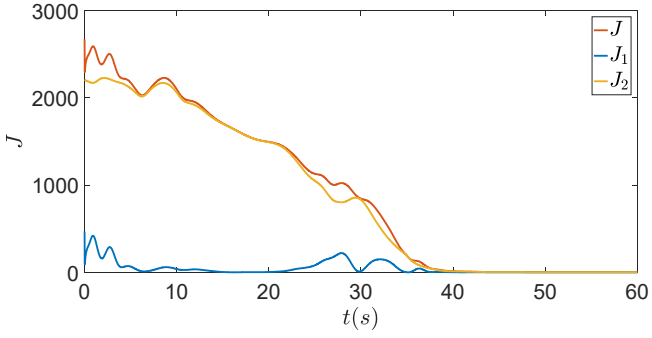

Fig. 10. The cost function in the simulation.

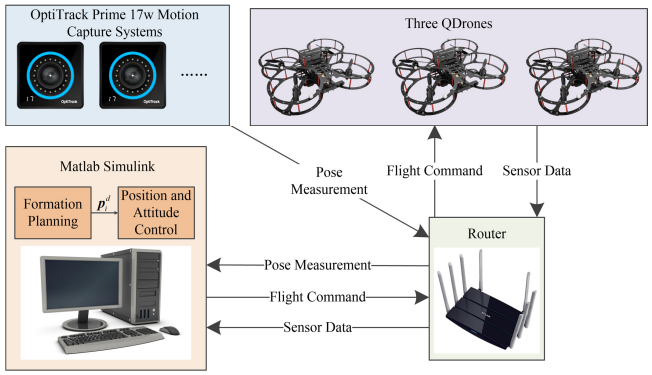

Fig. 11. The framework of experiment system and data flow.

The cost function during the transportation is also presented in Fig. 10. The cost function J is reduced over the whole. In some periods, J increases temporarily. The reason is that some new obstacle potential fields in the environment are activated during transportation to the transportation target.

The results of the simulation show that the team of four multirotor UAVs can collaboratively transport the payload through the obstacle area, and reach the transportation target in full-course flexible formations.

VI. Experiment

A. Experiment System Description

As shown in Fig. 1, the utilized UAVs are Quanser QDrone[1] with pose measurement from OptiTrack[2] Prime 17w motion capture systems. The framework of the physical experimental is presented in Fig. 11. Control PC, QDrones, and OptiTrack are all in the same LAN (Local Area Network) so that data transmission can be achieved via the Router.

B. Scenario

It is considered that three QDrone UAVs collaboratively transport a 0.39kg payload. The cables are 0.95m, 1.04m, and 0.61m in length, respectively. There is a static obstacle located on $\boldsymbol{q}_1 = \begin{bmatrix}0.1 & 0.8\end{bmatrix}^{\mathrm{T}}$m with radius 0.4m and a TurtleBot2[3] mobile robot as a dynamic obstacle initially located on $\boldsymbol{q}_2(0) = \begin{bmatrix}0.3083 & -0.8712\end{bmatrix}^{\mathrm{T}}$m with radius 0.23m. TurtleBot2 mobile robot would move in the negative direction of the x-axis. The take-off positions of UAVs are

$$\begin{cases}\boldsymbol{p}_1(0) = \begin{bmatrix}-1.7889 & -0.1266 & 0\end{bmatrix}^{\mathrm{T}}\mathrm{m}, \\ \boldsymbol{p}_2(0) = \begin{bmatrix}-1.6899 & -1.0471 & 0\end{bmatrix}^{\mathrm{T}}\mathrm{m}, \\ \boldsymbol{p}_3(0) = \begin{bmatrix}-0.5083 & 0.1137 & 0\end{bmatrix}^{\mathrm{T}}\mathrm{m}.\end{cases}$$

UAVs would climb to 1m forming an equilateral triangle formation, and start the transportation mission. The transportation target is $\boldsymbol{p}_t = \begin{bmatrix}1.5 & 0 & 1.2\end{bmatrix}^{\mathrm{T}}$m.

The parameters of formation planning were chosen as: $k_1 = 1$, $k_2 = 11$, $k_3 = 1$, and $c = 0.5$. The parameters for tracking

[1]https://www.quanser.com/products/qdrone/
[2]https://www.optitrack.com/
[3]https://www.turtlebot.com/turtlebot2/

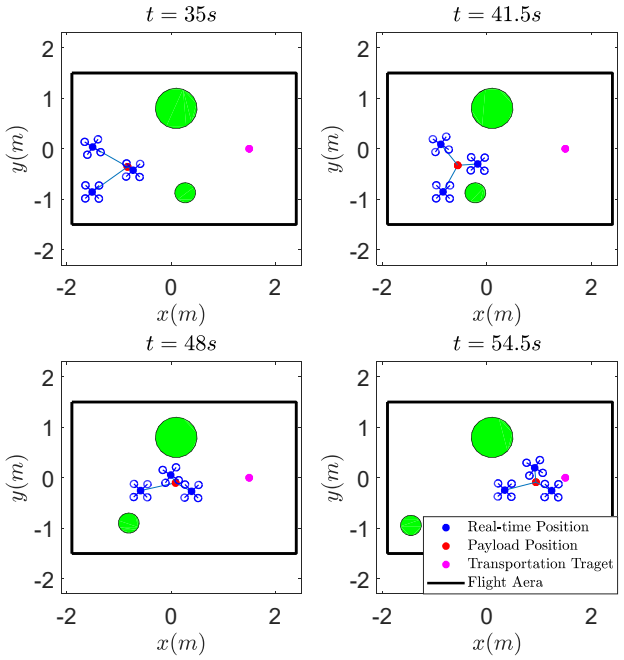

Fig. 12. The formation changes of UAVs during obstacles environment in the experiment.

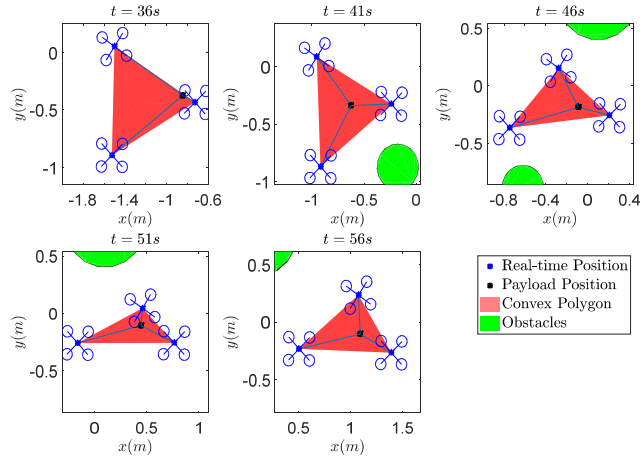

Fig. 13. The convex polygon of UAVs during obstacles environment in the experiment.

control are chosen as $\mathbf{K}_1(\dot{\boldsymbol{p}}_i) = \mathbf{K}_2(\dot{\boldsymbol{p}}_i) = 20\dot{\boldsymbol{p}}_i$, $\mathbf{C}_p = \mathbf{C}_a = diag(2,2,2)$, $\mathbf{R}_p = diag(1,0.8,0.8)$, and $\mathbf{R}_p = diag(5,5,5)$.

C. Experimental Results

As determined from the experimental results, the cooperative transportation mission starts at 35.5s, and multirotor UAVs arrive at the destination at 65s.

Fig. 12 and Fig 13 present the formation changes during the transportation mission. It is shown that the team of three multirotor UAVs shrinks the formation to cross the obstacle environment, and the oncoming dynamic obstacle TurtleBot2 is also avoided. The convex polygon consisting of UAVs is shown in Fig. 13. It can be found that the payload is

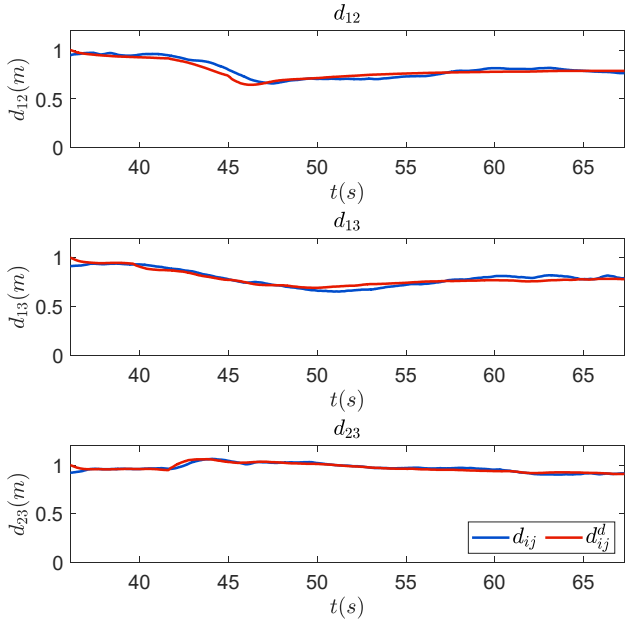

Fig. 14. The relative distance of UAVs in the experiment.

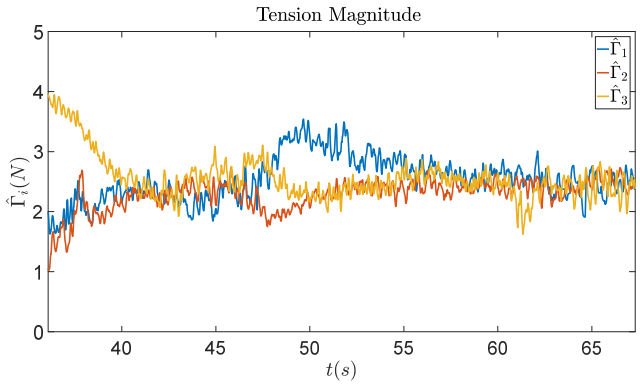

Fig. 15. The tension magnitude on cables in the experiment.

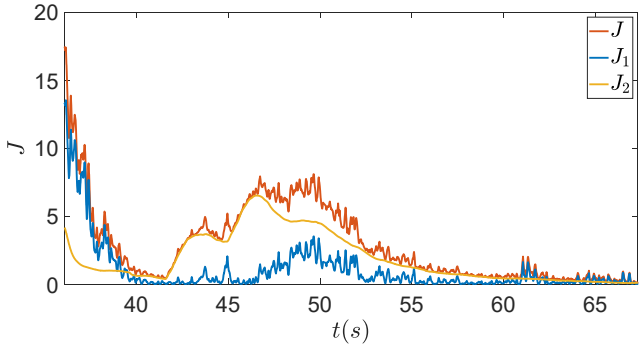

Fig. 16. The cost function in the experiment.

always inside the convex polygon, even though the payload is initially located at the boundary of the convex polygon (see the subgraph t=36s). At the initial time, there is also a large difference in the tension magnitude on cables (see Fig. 15). Under the proposed formation planning method, the gravity of the payload is quickly balanced to each cable. As shown in Fig. 14, similar to the simulation, UAVs always keep at a safe distance, and the individual UAVs track their desired position well, which demonstrates the effectiveness of the proposed position and attitude control.

The transportation process can be divided into three stages:

During the first period (35.5s-42s), multirotor UAVs hardly enter the potential field of obstacles. As tension magnitude shown in Fig. 15 and cost function in Fig. 16, J_1 decreases rapidly; meanwhile, the tension magnitude tends to reach a consensus.

Then, during the second period (42s-55s), multirotor UAVs are close to obstacles, and the potential fields of obstacles become active. Hence, there is an increase of J_2 in 42s-47s. Then, with the help of $\boldsymbol{F}_{2i}^d$, UAVs move away from obstacles; meanwhile, J_2 decrease again.

Finally, during the third period (55s-65s), obstacles are far away from UAVs, and the transportation target is about to arrive. J_2 tends to zero. The tension magnitude on cables is also balanced.

Throughout the entire transportation mission, the experimental results conform to the proposed formation criteria in Section III-A.

VII. Conclusion

This work proposed a real-time formation planning method for tethered multirotor UAV cooperative transportation in the condition of unknown payload and cable length. We proposed some formation criteria independent of the payload and cable length, and developed a corresponding optimization. This is the crucial step to solving the problem with unknown payload and cable length. A significant advantage of the proposed formation planning method is the ability to maintain tension on cables, which is not considered in those position-only-based formation planning methods. According to the simulated and experimental results, the cooperative transportation system can travel through the dynamic obstacle environment with flexible formations.

When the local minimum of the artificial potential functions occurs, we can design a series of sequential waypoints as transportation targets in the proposed formation planning methods.

The extension to distributed or decentralized formation planning method may be studied in future work. It would also be interesting to extend our method to a 6DOF rigidity payload.

Acknowledge

The authors would like to thank Prof. Qingkai Yang and Xianlin Zeng for their helpful discussions related to this work. We would also like to thank Chongxu Pei for his contribution to the experiments.

Appendix

A. Proof of Theorem 1

Define the tension estimation error as

$$\boldsymbol{\rho}_i = \begin{bmatrix} \boldsymbol{T}_i - \hat{\boldsymbol{T}}_i \\ \dot{\boldsymbol{T}}_i - \dot{\hat{\boldsymbol{T}}}_i \end{bmatrix},$$

According to (15), the derivative of error is:

$$\dot{\boldsymbol{\rho}}_i = \mathbf{L}\left(\dot{\boldsymbol{p}}_i\right)\boldsymbol{\rho}_i + \boldsymbol{\gamma}\ddot{\boldsymbol{T}}_i.$$

A Lyapunov function is considered as below

$$V_{Ti} = \frac{1}{2}\boldsymbol{\rho}_i^{\mathrm{T}}\boldsymbol{\rho}_i,$$

whose derivative is

$$\begin{aligned}\dot{V}_{Ti} =& \boldsymbol{\rho}_i^{\mathrm{T}}\left(\mathbf{L}\left(\dot{\boldsymbol{p}}_i\right)\boldsymbol{\rho}_i + \boldsymbol{\gamma}\ddot{\boldsymbol{T}}_i\right) \\ \leq& -\boldsymbol{\rho}_i^{\mathrm{T}}\left(-\mathbf{L}\left(\dot{\boldsymbol{p}}_i\right) - 0.5||\boldsymbol{\gamma}||_2\mathbf{I}_6\right)\boldsymbol{\rho}_i + 0.5\sigma_3^2.\end{aligned}$$

It is known $-\mathbf{L}\left(\dot{\boldsymbol{p}}_i\right) - 0.5||\boldsymbol{\gamma}||_2\mathbf{I}_6 > 0$. There the estimation error $\boldsymbol{\rho}_i$ is bounded.

B. Proof of Theorem 2

According to (1a)-(1c), it has

$$\ddot{\boldsymbol{p}}_i = \boldsymbol{f}\left(\boldsymbol{u}_i\right) + \boldsymbol{\delta}_i,$$

where

$$\boldsymbol{f}\left(\boldsymbol{u}_i\right) = \begin{bmatrix} u_{xi}u_{Fi}/m_i \\ u_{yi}u_{Fi}/m_i \\ u_{Fi}\cos\phi_i\cos\theta_i/m_i \end{bmatrix}, \quad \boldsymbol{\delta}_i = \begin{bmatrix} -T_{xi}/m_i \\ -T_{yi}/m_i \\ g - T_{zi}/m_i \end{bmatrix}.$$

The position tracking errors are defined as

$$\begin{aligned}\tilde{\boldsymbol{p}}_i =& \boldsymbol{p}_i^d - \boldsymbol{p}_i, \\ \dot{\tilde{\boldsymbol{p}}}_i =& \dot{\boldsymbol{p}}_i^d - \dot{\boldsymbol{p}}_i.\end{aligned}$$

The sliding mode surface can be denoted by

$$\boldsymbol{s}_{pi} = \mathbf{C}_p\tilde{\boldsymbol{p}}_i + \dot{\tilde{\boldsymbol{p}}}_i,$$

where $\boldsymbol{s}_{pi} = \begin{bmatrix} s_{xi} & s_{yi} & s_{zi} \end{bmatrix}^{\mathrm{T}}$.

We choose the following Lyapunov function $V_{pi} = \frac{1}{2}\boldsymbol{s}_{pi}^{\mathrm{T}}\boldsymbol{s}_{pi}$, whose derivative is

$$\begin{aligned}\dot{V}_{pi} =& \boldsymbol{s}_{pi}^{\mathrm{T}}\dot{\boldsymbol{s}}_{pi} \\ =& -\boldsymbol{s}_{pi}^{\mathrm{T}}\mathbf{R}_p\boldsymbol{s}_{pi} + \frac{1}{m_i}\boldsymbol{s}_{pi}^{\mathrm{T}}\tilde{\boldsymbol{T}}_i \\ \leq& -\boldsymbol{s}_{pi}^{\mathrm{T}}\left(\mathbf{R}_p - 0.5\mathbf{I}_3\right)\boldsymbol{s}_{pi} + \frac{1}{2m_i}\tilde{\boldsymbol{T}}_i^{\mathrm{T}}\tilde{\boldsymbol{T}}_i \\ \leq& -\boldsymbol{s}_{pi}^{\mathrm{T}}\left(\mathbf{R}_p - 0.5\mathbf{I}_3\right)\boldsymbol{s}_{pi} + \frac{1}{2m_i}\boldsymbol{\rho}_i^{\mathrm{T}}\boldsymbol{\rho}_i.\end{aligned}$$

Now a Lyapunov function including tension estimation errors is defined as below:

$$V_i = V_{pi} + V_{Ti} = \frac{1}{2}\boldsymbol{s}_{pi}^{\mathrm{T}}\boldsymbol{s}_{pi} + \frac{1}{2}\boldsymbol{\rho}_i^{\mathrm{T}}\boldsymbol{\rho}_i,$$

whose derivative is given by

$$\begin{aligned}\dot{V}_i =&\dot{V}_{pi} + \dot{V}_{Ti}\\ \leq& -\boldsymbol{s}_{pi}^{\mathrm{T}}\left(\mathbf{R}_p - 0.5\mathbf{I}_3\right)\boldsymbol{s}_{pi} + \frac{1}{2m_i}\boldsymbol{\rho}_i^{\mathrm{T}}\boldsymbol{\rho}_i\\ &-\boldsymbol{\rho}_i^{\mathrm{T}}\left(-\mathbf{L}\left(\dot{\boldsymbol{p}}_i\right) - 0.5||\boldsymbol{\gamma}||_2\mathbf{I}_6\right)\boldsymbol{\rho}_i + 0.5\sigma_3^2\\ \leq& -\boldsymbol{\rho}_i^{\mathrm{T}}\left(-\mathbf{L}\left(\dot{\boldsymbol{p}}_i\right) - 0.5||\boldsymbol{\gamma}||_2\mathbf{I}_6 - \frac{1}{2m_i}\mathbf{I}_6\right)\boldsymbol{\rho}_i + 0.5\sigma_3^2\\ &-\boldsymbol{s}_{pi}^{\mathrm{T}}\left(\mathbf{R}_p - 0.5\mathbf{I}_3\right)\boldsymbol{s}_{pi}\\ \leq& -\kappa_i V_i + C_i,\end{aligned}$$

where

$$\kappa_i = \min\left\{\begin{matrix}\lambda_{\min}\left(-\mathbf{L}\left(\dot{\boldsymbol{p}}_i\right) - 0.5||\boldsymbol{\gamma}||_2\mathbf{I}_6 - \frac{1}{2m_i}\mathbf{I}_6\right)\\ \lambda_{\min}\left(\mathbf{R}_p - 0.5\mathbf{I}_3\right)\end{matrix}\right\},$$

$$C_i = 0.5\sigma_3^2.$$

It implies that the position tracking error (e_{xi}, e_{yi}, e_{zi}) are stable under the position control (18).

C. Proof of Theorem 3

It is defined $\boldsymbol{\chi} = \begin{bmatrix}\phi_i & \theta_i & \psi_i\end{bmatrix}^{\mathrm{T}}$. According to (1d)-(1f), it has

$$\ddot{\chi}_i = \boldsymbol{h}\left(\dot{\boldsymbol{\chi}}_i\right) + \boldsymbol{\eta}\left(\boldsymbol{u}_i\right).$$

where

$$\boldsymbol{h}\left(\dot{\boldsymbol{\chi}}_i\right) = \begin{bmatrix}\dot{\theta}_i\dot{\psi}_i(I_y - I_z)/I_x\\ \dot{\psi}_i\dot{\phi}_i(I_z - I_x)/I_y\\ \dot{\phi}_i\dot{\theta}_i(I_x - I_y)/I_z\end{bmatrix}, \quad \boldsymbol{\eta}\left(\boldsymbol{u}_i\right) = \begin{bmatrix}\tau_{\phi i}/I_x\\ \tau_{\theta i}/I_y\\ \tau_{\psi i}/I_z\end{bmatrix}.$$

The attitude tracking errors are defined as

$$\begin{aligned}\tilde{\boldsymbol{\chi}}_i =&\boldsymbol{\chi}_i^d - \boldsymbol{\chi}_i,\\ \dot{\tilde{\boldsymbol{\chi}}}_i =&\dot{\boldsymbol{\chi}}_i^d - \dot{\boldsymbol{\chi}}_i.\end{aligned}$$

The sliding mode surface can be denoted by

$$\boldsymbol{s}_{ai} = \mathbf{C}_a\tilde{\boldsymbol{\chi}}_i + \dot{\tilde{\boldsymbol{\chi}}}_i,$$

where $\boldsymbol{s}_{ai} = \begin{bmatrix}s_{\phi i} & s_{\theta i} & s_{\psi i}\end{bmatrix}^{\mathrm{T}}$.

We choose the following Lyapunov function $V_{ai} = \frac{1}{2}\boldsymbol{s}_{ai}^{\mathrm{T}}\boldsymbol{s}_{ai}$, whose derivative is

$$\begin{aligned}\dot{V}_{ai} =&\boldsymbol{s}_{ai}^{\mathrm{T}}\dot{\boldsymbol{s}}_{ai}\\ =& -\boldsymbol{s}_{ai}^{\mathrm{T}}\mathbf{R}_a\boldsymbol{s}_{ai} \leq -2\lambda_{\min}\{\mathbf{R}_a\}V_{ai}.\end{aligned}$$

It implies $\boldsymbol{s}_{ai} \to \boldsymbol{0}$. Further, from $\boldsymbol{0} = \boldsymbol{s}_{ai} = \mathbf{C}_a\tilde{\boldsymbol{\chi}}_i + \dot{\tilde{\boldsymbol{\chi}}}_i$, we know that $\left(\tilde{\boldsymbol{\chi}}_i, \dot{\tilde{\boldsymbol{\chi}}}_i\right)$ will converge to $(\boldsymbol{0}, \boldsymbol{0})$.

REFERENCES

[1] H. Lee and H. J. Kim, "Trajectory tracking control of multirotors from modelling to experiments: A survey," *Int. J. Control Autom. Syst.*, vol.15, no.1, pp. 281-292, 2017.

[2] J. Gu, T. Su, Q. Wang, X. Du and M. Guizani, "Multiple Moving Targets Surveillance Based on a Cooperative Network for Multi-UAV," *IEEE Commun. Mag.*, vol. 56, no. 4, pp. 82-89, Apr. 2018.

[3] A. Wallar, E. Plaku and D.A. Sofge, "Reactive Motion Planning for Unmanned Aerial Surveillance of Risk-Sensitive Areas," *IEEE Trans. Autom. Sci. Eng.*, vol. 12, no. 3, pp. 969-980, Jul. 2015.

[4] R. Skulstad, C. Syversen, M. Merz, N. Sokolova, T. Fossen and T. Johansen, "Autonomous net recovery of fixed- wing UAV with single-frequency carrier-phase differential GNSS," *IEEE Aerosp. Electron. Syst. Mag.*, vol. 30, no. 5, pp. 18-27, May 2015.

[5] K. Klausen, T.I. Fossen and T.A. Johansen, "Autonomous recovery of a fixed-wing UAV using a net suspended by two multirotor UAVs," *J. Field Robot.*, vol. 35, no. 5, pp. 717-731, 2018.

[6] K. Harikumar, J. Senthilnath and S. Sundaram, "Multi-UAV Oxyrrhis Marina-Inspired Search and Dynamic Formation Control for Forest Firefighting," *IEEE Trans. Autom. Sci. Eng.*, vol. 16, no. 2, pp. 863-873, Apr. 2019.

[7] W. Shang, B. Zhang, B. Zhang, F. Zhang and S. Cong, "Synchronization Control in the Cable Space for Cable-Driven Parallel Robots," *IEEE Trans. Ind. Electron.*, vol. 66, no. 6, pp. 4544-4554, June 2019.

[8] N. Michael, J. Fink, and V. Kumar, "Cooperative manipulation and transportation with aerial robots," *Auton. Robot.*, vol. 30, no.1, pp. 73-86, Jan. 2011.

[9] C. Masone, H. H. Blthoff and P. Stegagno, "Cooperative transportation of a payload using quadrotors: A reconfigurable cable-driven parallel robot," in *Proc. IEEE/RSJ Int. Conf. Intell. Robots Syst.*, Oct. 2016, pp. 1623-1630.

[10] Z. Li, J. Horny, J. Langelaanz, "Coordinated transport of a slung load by a team of autonomous rotorcraft", in *AIAA Guid., Navig. Control Conf.*,Jan, 2014.

[11] J. Geng and J. W. Langelaan, "Cooperative Transport of a Slung Load Using Load-Leading Control", *J. Guid. Control Dyn.*, vol. 43, no. 7, pp. 1313-1331, 2020.

[12] S. Thapa, R. V. Self, R. Kamalapurkar and et al., "Cooperative Manipulation of an Unknown Payload With Concurrent Mass and Drag Force Estimation," *IEEE Control Syst. Lett.*, vol. 3, no. 4, pp. 907-912, Oct. 2019.

[13] S. Thapa, Bai H, Acosta J , "Force Control in Cooperative Aerial Manipulation," in *Proc. Int. Conf. Unmanned Aircr. Syst.*, Jun. 2018, pp. 1302-1309.

[14] T. Lee, K. Sreenath, V. Kumar, "Geometric Control of Cooperating Multiple Quadrotor UAVs with a Suspended Payload," in *Proc. 52nd IEEE Conf. Decis. Control.*, Dec. 2013, pp. 5510-5515.

[15] T. Lee, "Geometric Control of Multiple Quadrotor UAVs Transporting a Cable-Suspended Rigid Body," in *Proc. 53nd IEEE Conf. Decis. Control.*, Dec. 2014, pp. 6155-6160.

[16] T. Lee, "Geometric Control of Quadrotor UAVs Transporting a Cable-Suspended Rigid Body," *IEEE Trans. Control Syst. Technol.*, vol. 26, no. 1, pp. 255-264. 2018.

[17] Markus Bernard. "Autonomous Transportation and Deployment with Aerial Robots for Search and Rescue Missions," *J. Field Robot.*, vol. 28, no 6, pp. 914-931, 2011.

[18] K. Klausen, C. Meissen, T.I. Fossen, M. Arcak and T.A. Johansen, "Cooperative Control for Multirotors Transporting an Unknown Suspended Load Under Environmental Disturbances," *IEEE Trans. Control Syst. Technol.*, vol. 28, no. 2, pp. 653-660, Mar. 2020.

[19] X. Zhang, F. Zhang, P. Huang et al., "Self-Triggered Based Coordinate Control with Low Communication for Tethered Multi-UAV Collaborative Transportation," *IEEE Robot. Autom. Lett.*, vol. 6, no. 2, pp. 1559-1566, 2021.

[20] K. Mohammadi, S. Sirouspour and A. Grivani, "Control of Multiple Quad-Copters With a Cable-Suspended Payload Subject to Disturbances," *IEEE/ASME Trans. Mechatron.*, vol. 25, no. 4, pp. 1709-1718, Aug. 2020.

[21] Y. Liu, F. Zhang, P. Huang, and X. Zhang, "Analysis, planning and control for cooperative transportation of tethered multi-rotor UAVs," *Aerosp. Sci. Technol.*, vol. 113, p. 106673, Jun. 2021.

[22] H. G. d. Marina and E. Smeur, "Flexible collaborative transportation by a team of rotorcraft," in *Proc. Int. Conf. Robot. Autom.*, May 2019, pp. 1074-1080.

[23] S. Heshmati-Alamdari, C. P. Bechlioulis, G. C. Karras, and K. J. Kyriakopoulos, "Cooperative Impedance Control for Multiple Underwater Vehicle Manipulator Systems Under Lean Communication," *IEEE J. Ocean. Eng.*, vol. 46, no. 2, pp. 447-465, Apr. 2021.

[24] A. Tagliabue, M. Kamel, S. Verling and et al., "Collaborative Transportation Using MAVs via Passive Force Control," in *Proc. Int. Conf. Robot. Autom.*, May 2017, pp. 5766-5773.

[25] S. Barawkar, M. Radmanesh, M. Kumar and et al., "Fuzzy Logic based Variable Damping Admittance Control for Multi-UAV Collaborative Transportation," in *Proc. Am. Control Conf.*, Jun. 2018, pp. 2084-2089.

[26] A. Tagliabue, M. Kamel, R. Siegwart, and J. Nieto, "Robust collaborative object transportation using multiple MAVs," *Int. J. Robot. Res.*, vol. 38, no. 9, pp. 1020-1044, Aug. 2019.

[27] C. Gabellieri, M. Tognon, D. Sanalitro, L. Pallottino and A. Franchi, "A study on force-based collaboration in swarms," *Swarm Intell.*, vol. 14, no. 1, pp. 57-82, Mar. 2020.

[28] I. H. B. Pizetta, A. S. Brando and M. Sarcinelli-Filho, "Avoiding obstacles in cooperative load transportation," *ISA Trans.*, vol. 91, pp. 253-261, Aug. 2019.

[29] J.Gimenez, D. C. Gandolfo, L. R. Salinas, Cl. Rosales and R. Carelli, "Multi-objective control for cooperative payload transport with rotorcraft UAVs," *ISA Trans.*, vol. 80, pp. 491-502, Sep. 2018.

[30] H. Lee, H. Kim, and H. J. Kim, "Planning and Control for Collision-Free Cooperative Aerial Transportation," *IEEE Trans. Autom. Sci. Eng.*, vol. 15, no. 1, pp. 189-201, Jan. 2018.

[31] A. Hegde and D. Ghose, "Multi-UAV Collaborative Transportation of Payloads with Obstacle Avoidance," *IEEE Control Syst. Lett.*, vol. 6, no. 1, pp. 926-931, 2022.

[32] B. E. Jackson, T. A. Howell, K. Shah, M. Schwager and Z. Manchester, "Scalable Cooperative Transport of Cable-Suspended Loads With UAVs Using Distributed Trajectory Optimization," *IEEE Robot. Autom. Lett.*, vol. 5, no. 2, pp. 3368-3374, Apr. 2020.

[33] G. Tartaglione, E. DAmato, M. Ariola, P. S. Rossi and T. A. Johansen, "Model predictive control for a multi-body slung-load system," *Robot. Auton. Syst.*, vol. 92, pp. 1-11, Jun. 2017.

[34] S. Bouabdallah, P. Murrieri and R. Siegwart, "Design and Control of an Indoor Micro Quadrotor," in *Proc. Int. Conf. Robot. Autom.*, Apr. 2004, pp. 4393-4398.

[35] M. Labbadi and M. Cherkaoui, "Adaptive Fractional-Order Nonsingular Fast Terminal Sliding Mode Based Robust Tracking Control of Quadrotor UAV with Gaussian Random Disturbances and Uncertainties," *IEEE Trans. Aerosp. Electron. Syst.*, vol. 57, no. 4, pp. 2265-2277, 2021.

[36] S. J. Lee and H. J. Kim, "Autonomous swing-angle estimation for stable slung-load flight of multi-rotor UAVs," in *Proc. IEEE Int. Conf. Robot. Autom.*, May 2017 pp. 4576-4581.

[37] M. Chen, S. Xiong, and Q. Wu, "Tracking Flight Control of Quadrotor Based on Disturbance Observer," *IEEE Trans. Syst. Man, Cybern. Syst.*, vol. 51, no. 3, pp. 1414-1423, 2021.

[38] K. K. Dhiman, M. Kothari, and A. Abhishek, "Autonomous load control and transportation using multiple quadrotors," *J. Aerosp. Inf. Syst.*, vol. 17, no. 8, pp. 417-435, Aug. 2020.

[39] A. Petitti, D. Sanalitro, M. Tognon, A. Milella, J. Cortes, and A. Franchi, "Inertial Estimation and Energy-Efficient Control of a Cable-suspended Load with a Team of UAVs," in *Proc. of Int. Conf. Unmanned Aircr. Syst.*, pp. 158-165, 2020.

[40] D. A. Lawrence, "Impedance control stability properties in common implementations," in *Proc. Int. Conf. Robot. Autom.*, Apr. 1988, pp. 1185-1190.

[41] C. Ott, R. Mukherjee and Y. Nakamura, "Unified impedance and admittance control," in *Proc. Int. Conf. Robot. Autom.*, May. 2010, pp.554-561.

[42] M. Mesbahi and M. Egerstedt, *Graph Theoretic Methods in Multi-Agent Networks.* Princeton, NJ, USA: Princeton Univ. Press, 2010.

[43] R. Olfati-Saber, J. A. Fax, and R. M. Murray, "Consensus and cooperation in networked multi-agent systems," *Proc. IEEE*, vol. 95, no. 1, pp. 215-233, 2007.

[44] J. Erskine, A. Chriette, and S. Caro, "Wrench Analysis of Cable-Suspended Parallel Robots Actuated by Quadrotor Unmanned Aerial Vehicles," *J. Mech. Robot.*, vol. 11, no. 2, 2019.

[45] J. Erskine, A. Chriette, and S. Caro, "Control and configuration planning of an aerial cable towed system," in *Proc. IEEE Int. Conf. Robot. Autom.*, May 2019, pp. 6440-6446.

[46] F. E. Udwadia and R. E. Kalaba, "What is the general form of the explicit equations of motion for constrained mechanical systems?," *J. Appl. Mech. Trans. ASME*, vol. 69, no. 3, pp. 335-339, May 2002.

[47] B. Shirani, M. Najafi and I. Izadi, "Cooperative load transportation using multiple UAVs," *Aerosp. Sci. Technol.*, vol. 84, pp. 158-169, Jan. 2019.

[48] M. Chen, "Robust tracking control for self-balancing mobile robots using disturbance observer," *IEEE/CAA J. Automatica Sin.*, vol. 3, no.4, pp. 458-465, Jul. 2017.

Xiaozhen Zhang received B.S. degree in navigation, guidance and control, from Northwestern Polytechnical University, Xian, China, in 2021. He is currently working toward the Ph.D. degree in control engineering at Beijing Institute of Technology, Beijing, China.

His research interests include robotics, formation planning, formation control and multi-agent systems.

Zhang Fan (M 18, S 16) received M.S. and Ph.D. in Navigation, Guidance and Control, form School of Astronautics, Northwestern Polytechnical University in 2012 and 2017 respectively, and received B.S. in Detection, Guidance and Control Technology in 2009. She is currently an associate research professor in School of Astronautics, Northwestern Polytechnical University.

Her research focuses on the dynamic and control of tethered robot and intelligent control of multi-agent system.

Panfeng Huang (M 06, SM18) received B.S. and M.S. degree from Northwestern Polytechnical University in 1998, 2001, respectively, and Ph.D. from the Chinese University of Hong Kong in the area of Automation and Robotics in 2005. He is currently a Professor of School of Astronautics and Vice Director of Research Center for Intelligent Robotics at the Northwestern Polytechnical University.

His research interests include tethered space robotics, intelligent control, machine vision, and space teleoperation.